Nano Research
2022, 15(5): 3913–3919

ISSN 1998-0124 CN 11-5974/O4
https://doi.org/10.1007/s12274-021-4046-z

Ultrafast Joule heating synthesis of hierarchically porous graphene-based Co-N-C single-atom monoliths

Lingli Xing, Rui Liu, Zhichao Gong, Jingjing Liu, Jianbin Liu, Haisheng Gong, Kang Huang, and Huilong Fei (✉)

Advanced Catalytic Engineering Research Center of the Ministry of Education, State Key Laboratory for Chemo/Biosensing and Chemometrics, and College of Chemistry and Chemical Engineering, Hunan University, Changsha 410082, China

Received: 6 November 2021 / **Revised:** 2 December 2021 / **Accepted:** 4 December 2021

ABSTRACT

Herein, we develop a transient heating-quenching strategy triggered by Joule heating for the synthesis of single-atom cobalt- and nitrogen-doped graphene materials with three-dimensional porous monolithic architecture (denoted as CoNG-JH). The ultrafast Joule heating procedure simultaneously enables the reduction of graphene oxide and the incorporation of metal and nitrogen atoms into the graphene matrix within 2-second period. Meanwhile, the transient quenching avoids the extended heating-induced atom aggregation, ensuring the rapid and stable dispersion of atomic-scale CoN_x active sites in graphene. Additionally, the interconnected macropores and nanopores formed by the self-assembly of graphene sheets facilitate the unimpeded ion and gas transport during the catalytic process. When used as an electrode for the hydrogen evolution reaction (HER), the fabricated free-standing CoNG-JH exhibits high catalytic activity and durability with a low overpotential of 106 mV at 10 $\mathrm{mA\cdot cm^{-2}}$ and a small Tafel slope of 66 $\mathrm{mV\cdot dec^{-1}}$ in 0.5 M H_2SO_4 electrolyte. The presented synthesis and design strategy open up a rapid and facile route for the manufacturing of single atom catalysts.

KEYWORDS

Joule heating, single atom catalysts, hierarchically porous structure, self-supporting film, hydrogen evolution reaction

1 Introduction

Single-atom catalysts (SACs), as a new frontier in catalysis, have attracted worldwide research attention due to the unique coordination environments and maximized atom-utilization efficiency [1–3]. Recently, SACs have been deeply developed to achieve high-efficiency activity in energy-related conversion applications with different strategies, such as electronic metal-support interaction (EMSI), adjacent atomic modulation effect, support-defect engineering strategy and so on [4–7]. On the other hand, graphene, with large surface area, excellent (electro-) chemical stability and high electrical conductivity, has been extensively employed to support metal single atoms to prevent atom aggregation originated from high surface free energy [8]. To further tailor the physicochemical properties of graphene, substitutional doping with heteroatoms (N, P, S, etc.) is proved as a versatile means to endow graphene with extended performance and abundant anchoring sites for SACs [9, 10]. As a unique class of SACs, atomically dispersed transition metals embedded in nitrogen-doped graphene-like carbons (M-N-Cs) have been identified as the most promising alternative to precious-metal-based materials in electrocatalytic applications, including the technologically important hydrogen evolution reaction (HER) [11, 12]. Nevertheless, extensive efforts are required to explore new synthetic strategies toward M-N-C materials and further improve their electrocatalytic performance in order to address the challenges in practical applications.

In terms of the synthesis of M-N-Cs, the pyrolysis treatment at high temperature is the most widely adopted approach to achieving the co-doping of metal and nitrogen atoms in graphene matrix [13–16]. However, the pyrolysis process usually takes tens of minutes to several hours, which is not only time- and energy-consuming, but also tends to induce the aggregation of metal atoms [17]. Thus, it is necessary to seek a rapid and facile strategy with prospect of industrial application to synthesize M-N-Cs. Recently, Hu et al. fabricated a series of uniform, high-density and size-controllable multimetallic nanoparticles via an ultrafast carbothermal shockwave process triggered by Joule heating with the flash heating and cooling capability (ramp rates up to the order of 10^5 $\mathrm{K\cdot s^{-1}}$) [18–21]. Taking a step further, they synthesized single-atom dispersed Pt-C materials with superior thermal stability via the transient high-temperature pulse technique [22]. The high-temperature heating process can provide the activation energy for the dispersion of metal atoms on the substrates, while the rapid quenching process can prevent the extended heating-induced atom aggregation.

In general, M-N-Cs were prepared in powdery form and thus polymer binders would be inevitably introduced during the process of preparing electrodes for electrocatalytic measurements, which could impede mass transport and block exposed active sites, leading to unsatisfactory performance [23, 24]. To this end, constructing self-supporting monolithic M-N-C electrodes could circumvent the problems encountered in traditional slurry-based electrodes [25, 26]. Additionally, the HER process occurs at the solid-liquid-gas triple-phase interfaces, including surface reaction, electron transfer and mass diffusion [27]. Thus, exposing more

---

Address correspondence to hlfei@hnu.edu.cn

active sites to the interfaces has become a key design principle of high-performance M-N-C electrodes [28]. Further, introducing porous structures to the self-supporting electrode is of vital importance to improve mass transport efficiency and enhance the utilization efficiency of the active sites in M-N-C materials [12, 29]. Particularly, macroporous skeleton structures can reduce the tortuosity of the electrode and facilitate the mass transfer of reactants (protons) and products (hydrogen gases) during the HER process [30, 31].

Herein, we employed an ultrafast Joule heating approach to synthesizing a self-supporting and porous M-N-C single-atom monolith. As a typical demonstration, the Co-N-C sites integrated into the porous graphene-based monoliths (CoNG-JH) were achieved via a hydrothermal self-assembly process and a transient Joule heating technique. With the 2-second Joule heating technique, the nitrogen and cobalt atoms are efficiently co-embedded into the defect sites of graphene along with the reduction of graphene oxide (GO), and the transient quenching avoids the extended heating-induced atom aggregation, ensuring the rapid and stable dispersion of atomic-scale CoN_x active sites in graphene. The three-dimensional interconnected macropores and nanopores constructed by entangled graphene sheets facilitate electrolyte penetration, ion diffusion and gas removal during the HER process. When directly used as an electrode for catalyzing the HER, the monolithic CoNG-JH exhibits a low overpotential of 106 mV to reach a current density of 10 $mA \cdot cm^{-2}$, a small Tafel slope of 66 $mV \cdot dec^{-1}$ and long-term durability in 0.5 M H_2SO_4 electrolyte.

2 Results and discussion

2.1 Synthesis and structural characterization

Figure 1 illustrates the synthesis procedure of the self-supported porous CoNG-JH film and the designed advantageous features for the HER process. Briefly, GO precursor was firstly reacted with aqueous ammonia to form the amine-functionalized GO (AGO), which can provide nitrogen doping sources in the following step. Then, controlled amounts of cobalt salts and ethanol were introduced into AGO solution, which was hydrothermally self-assembled into the Co^{2+}-containing AGO (CoAGO) hydrogel. The introduction of ethanol as co-solvent can affect the crystallization behavior of ice growth by decreasing the freezing point during the ice-templated freezing treatment. The monolithic CoAGO hydrogel with desired thickness was freeze-dried to form CoAGO aerogel with hierarchically porous architecture. Subsequently, the aerogel film was subjected to electrically-triggered 2-second Joule heating process under NH_3 atmosphere. NH_3 was introduced as secondary nitrogen doping source besides the amino groups from AGO. The high-energy environment from Joule heating could provide the activation energy for the dispersion of metal atoms, the removal of oxygen functional groups in GO and the ejection of carbon atoms as CO_2 or CO with the formation of defects [32]. The defects in graphene as excellent anchoring sites could coordinate with N and Co atoms to form the Co-N-C sites integrated into graphene to finally achieve CoNG-JH. Furthermore, the instantaneous quenching could avoid the extended heating-induced atom aggregation, thus ensuring the stable existence of the single-atom CoN_x moieties in graphene. As control samples, NG-JH and CoG-JH were prepared following the same synthetic procedure of CoNG-JH except that no cobalt salts or nitrogen sources were introduced, respectively.

The morphology, pore structure and compositions of the as-prepared monolithic films were investigated by different characterization techniques, as shown in Fig. 2. Top-view and cross-section scanning electron microscopic (SEM) images show the three-dimensional interconnected macroporous skeleton structures of CoNG-JH and the diameter of the macropores ranges from 10 μm to 20 μm (Figs. 2(a) and 2(b)). The inset optical image in Fig. 2(a) displays the monolithic film of CoNG-JH. Transmission electron microscopic (TEM) images show that the macroporous wall structure of CoNG-JH consisting of entangled graphene sheets (Fig. 2(c) and Fig. S1 in the Electronic Supplementary Material (ESM)). In addition, no Co aggregates were observed in TEM images at different magnifications,

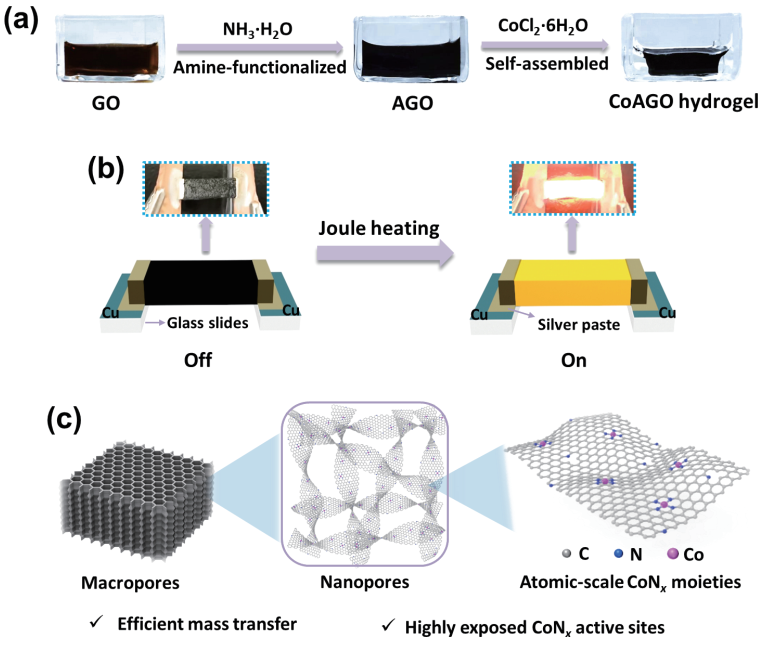

Figure 1 Fabrication of the monolithic porous CoNG-JH film by self-assembly and Joule heating. (a) Schematic of the preparation procedure of the self-supported CoAGO hydrogels: amino-functionalization of GO, adding cobalt salts, and hydrothermally self-assembled into hydrogels. (b) Schematic of the electrical Joule heating process of CoAGO aerogel films: heating/quenching was realized instantaneously with on/off status. (c) Design strategy of CoNG-JH electrode for hydrogen production: macropores and nanopores created by the self-assembly of graphene sheets can effectively promote mass transport and expose more active sites to the HER interfaces; ultrafast Joule heating ensures the rapid formation of atomic CoN_x moieties and avoids the generation of nanoparticles.

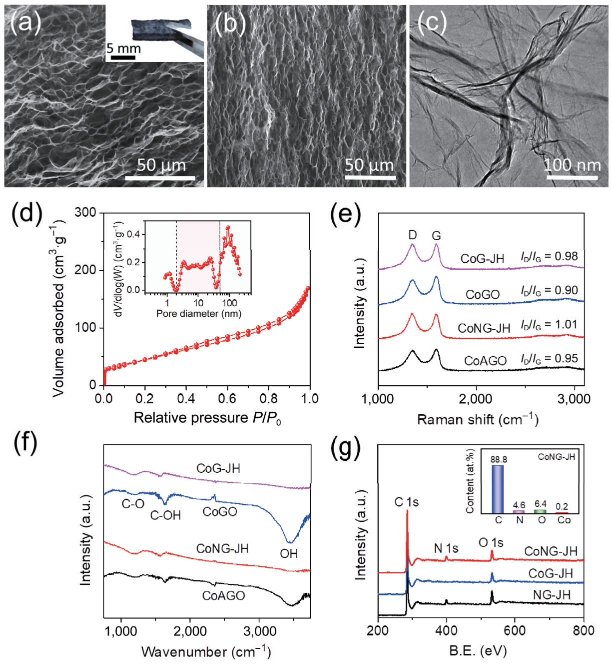

Figure 2 Characterization of the morphology, porous structure and compositions. (a) and (b) Top-view and cross-section SEM images of CoNG-JH, showing the interconnected macroporous skeleton structures. The inset shows the optical image of the monolithic CoNG-JH film. (c) TEM image of CoNG-JH, showing the wall structure formed by entangled graphene sheets. (d) Nitrogen adsorption and desorption curves of CoNG-JH. The inset shows the pore-size distribution curve of CoNG-JH. (e) Raman spectra of CoNG-JH, CoG-JH, CoAGO and CoGO. (f) FT-IR spectra of CoNG-JH, CoG-JH, CoAGO and CoGO. (g) XPS survey spectra of CoNG-JH and control samples (CoG-JH and NG-JH). The inset chart shows the atomic percentages of carbon, nitrogen, oxygen and cobalt in CoNG-JH measured by XPS.

indicating that Co atoms may be atomically dispersed on graphene sheets. Nitrogen adsorption and desorption analysis was carried out to investigate the porosity of CoNG-JH. CoNG-JH possesses a Brunauer-Emmett-Teller (BET) specific surface area of 203 m^2·g^{-1} and exhibits the type-IV isotherm with a hysteresis loop, implying the existence of abundant mesopores (Fig. 2(d)) [33–35]. Pore-size distribution curve reveals the multi-scale porosity of CoNG-JH with the coexistence of micropores, mesopores and macropores, as shown in the inset of Fig. 2(d) [36]. The electrochemical surface area (ECSA) was estimated by measuring the double-layer capacitance (C_{dl}) (Fig. S2 in the ESM). CoNG-JH exhibits a significantly higher C_{dl} of 86 mF·cm^{-2} than that of powdered catalysts [37, 38], which confirms the role of hierarchically porous architecture in the exposure of electrochemically active interfaces. Within the three-dimensional hierarchically porous architecture, the graphene sheets serve as the supports for dispersing single-atom CoN$_x$ sites, while the macroporous skeleton and nanopores provide the interconnected highway to transport the reactants (protons) and products (hydrogen gases).

Raman spectra in Fig. 2(e) exhibit the disorder-induced D-band at 1,345 cm^{-1} and graphitic carbon-related G-band at 1,585 cm^{-1} [39, 40]. The I_D-to-I_G ratio of CoNG-JH and CoG-JH is higher than CoAGO and CoGO precursors before Joule heating, suggesting that the ultrafast Joule heating process promoted the generation of defect sites, which could serve as anchoring sites for single-atom Co-N-C moieties. Fourier-transform infrared spectroscopy (FT-IR) spectra were measured to probe the structural changes induced by Joule heating, as shown in Fig. 2(f). The number of oxygen-containing functional groups in CoAGO and CoGO precursors was significantly decreased after transforming to CoNG-JH and CoG-JH, which manifests the high efficiency of the 2-second Joule heating in the reduction of graphene oxide. The compositions of CoNG-JH and control catalysts were investigated by X-ray photoelectron spectroscopy (XPS). The XPS survey spectra reveal the presence of C, N and O elements and the peak intensity of Co is negligible due to its low content (Fig. 2(g)). CoNG-JH consists of 88.8 at.% C, 4.6 at.% N, 6.4 at.% O and 0.2 at.% Co, as summarized in the inset of Fig. 2(g). The content of Co element for CoNG-JH was further determined to be ~ 0.81 wt.% by inductively coupled plasma mass spectrometry (ICP-MS).

2.2 Analysis of composition, chemical state and atomic structure

To further study the composition of the monolithic Co-N-C materials, X-ray diffraction (XRD) measurements were performed. Figure 3(a) shows two characteristic peaks at 25.8° and 42.5° belonging to (002) and (100) planes of graphitic carbon for CoNG-JH with different Co contents. There existed a weak diffraction peak at 44.2° belonging to (111) plane of Co crystal for 1.5CoNG-JH (that was prepared with 1.5 times as high as Co feeding ratio during preparation compared to the optimal sample) [41], while no diffraction peaks indexed to Co crystal were observed in CoNG-JH. The XRD results suggest that the cobalt species in CoNG-JH are highly dispersed in graphene sheets and the excessive addition of Co precursor can promote the formation of Co nanoparticles. The chemical states of CoNG-JH and control catalysts (NG-JH and CoG-JH) were probed by the high-resolution XPS spectra. The XPS C 1s and O 1s spectra of CoNG-JH were provided in Fig. S3 in the ESM. The XPS N 1s spectra in Fig. 3(b) were deconvoluted into four peaks arising from N-Co/pyridinic N (398.5 eV), pyrrolic N (400.1 eV), graphitic N (401.5 eV) and oxidized N (403.2 eV) [42]. It is noted that the content of N-Co/pyridinic N in CoNG-JH is significantly higher than that of NG-JH, indicating the formation of CoN$_x$ moieties in CoNG-JH. Moreover, the chemical state of Co element in CoNG-JH and 1.5CoNG-JH was probed by the XPS Co 2p spectra (Fig. 3(c)). There existed two dominant peaks at 780.5 and 795.9 eV for CoNG-JH, corresponding to the Co 2p$_{3/2}$ and 2p$_{1/2}$ levels, respectively, which can be ascribed to the atomically dispersed CoN$_x$ moieties [28, 43]. A shift to lower binding energy of Co 2p$_{3/2}$ and 2p$_{1/2}$ peaks was observed for 1.5CoNG-JH, indicating the formation of metallic Co, in agreement with the XRD results [44]. The atomic-resolution annular dark-field scanning transmission electron microscopic (ADF-STEM) images clearly reveal that the isolated Co atoms (bright dots) with size of ~ 2 Å disperse individually in CoNG-JH (Figs. 3(d) and 3(e)). The elemental mapping images in Fig. 3(f) show that the C, N and Co elements distribute uniformly over the graphene sheets in CoNG-JH. Combining the results of TEM, XRD, XPS and ADF-STEM, CoNG-JH synthesized via the ultrafast Joule heating technique has atomically dispersed CoN$_x$ moieties integrated into the graphene sheets without Co aggregates.

2.3 Electrocatalytic performance toward HER

The HER activities were evaluated in a standard three-electrode configuration in 0.5 M H_2SO_4 electrolyte. The monolithic CoNG-JH film was directly used as working electrode without the addition of conductive additive or polymer binder, greatly simplifying the electrode preparation process. All polarization curves were subjected to background and *iR* correction, as illustrated in Fig. S4 in the ESM [45]. The optimal CoNG-JH electrode has an average areal mass loading of 1.0 mg·cm^{-2} with a thickness of 1.5–2 mm (Fig. S5 in the ESM). Optimization on the Co content indicates that the atomically dispersed CoN$_x$ moieties play a dominant role in the HER and the excessive addition of Co would not lead to further increase in catalytic performance (Fig. S6

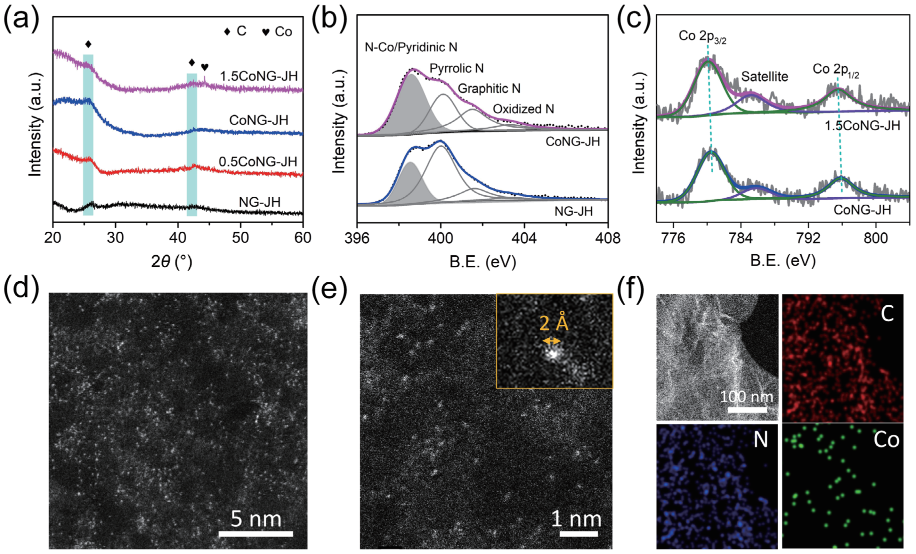

Figure 3 Analysis of composition, chemical state and atomic structure. (a) XRD patterns of the monolithic Co-N-C materials with different cobalt contents for NG-JH, 0.5CoNG-JH, CoNG-JH and 1.5CoNG-JH. (b) XPS N 1s spectra of CoNG-JH and NG-JH. (c) XPS Co 2p spectra of CoNG-JH and 1.5CoNG-JH. (d) and (e) ADF-STEM images at different magnifications for CoNG-JH, showing that the single Co atoms well dispersed in the carbon matrix. The inset in (e) shows an individual Co atom with the size of ~ 2 Å. (f) STEM image and corresponding elemental mapping images of CoNG-JH.

in the ESM). The effect of Joule heating atmosphere (Ar versus NH_3) on HER activity was studied (Fig. S7 in the ESM). For the preparation of CoNG-JH, NH_3 was introduced in the Joule heating atmosphere as secondary nitrogen doping source in addition to the amino groups of AGO to facilitate the generation of more electro-active CoN_x sites, resulting in higher HER activity than control samples prepared with solo/no nitrogen source. Figure 4(a) shows the polarization curves of CoNG-JH and control catalysts (CoG-JH and NG-JH), along with the commercial Pt/C as reference. It is notable that CoNG-JH requires a significantly smaller overpotential (η) of 106 mV to deliver a current density of 10 mA·cm^{-2} than NG-JH (η_{10} = 422 mV) and CoG-JH (η_{10} = 366 mV), indicating the critical role of the atomically dispersed CoN_x active sites in CoNG-JH [46, 47]. Additionally, the facilitated reaction kinetics of CoNG-JH is further manifested by the electrochemical impedance spectroscopy (EIS), revealing that it has a lower charge transfer resistance in comparison with CoG-JH and NG-JH (Fig. S8 in the ESM). Benefiting from the hierarchically porous architecture, the self-supporting CoNG-JH electrode exhibits a higher activity than CoNG-JH-slurry electrode (η_{10} = 170 mV) prepared by conventional drop-casted method due to the improvement of mass transfer efficiency (Fig. S9 in the ESM). The monolithic CoNG-JH electrode exhibits superior HER activity compared with the state-of-the-art Co-based SACs reported recently (Fig. 4(b) and Table S1 in the ESM), such as Co-SAs/PTF-600 (η_{10} = 94 mV) [48], Co-P_1N_3 (η_{10} = 98 mV) [49], Co/NCNT/NG (η_{10} = 123 mV) [38], CoNG-Cl (η_{10} = 130 mV) [50], Co-SAS/HOPNC (η_{10} = 137 mV) [51], Co-NG-5010-10 (η_{10} = 146 mV) [52], Co-NG (η_{10} = 147 mV) [42], and Co-NG-MW (η_{10} = 175 mV) [17]. The Tafel slopes for CoNG-JH, CoG-JH, NG-JH and commercial Pt/C were determined from the polarization curves in Fig. 4(a) and CoNG-JH exhibits a smaller Tafel slope of 66 mV·dec^{-1} compared with control catalysts (Fig. 4(c)). Moreover, turnover frequency (TOF) was estimated by assuming each Co center as one active site to assess the intrinsic activity of CoNG-JH, as illustrated in Fig. 4(d). CoNG-JH, with the TOF values of 0.36 s^{-1} at η = 100 mV and 1.18 s^{-1} at η = 150 mV, exhibits comparable intrinsic activity with previously reported catalysts, such as Co-NG (0.1 s^{-1} at η = 100 mV) [42], Co-NG-MW (0.38 s^{-1} at η = 100 mV) [17], Co-SAS/HOPNC (0.41 s^{-1} at η = 100 mV) [51], Co-P_1N_3 (1.6 s^{-1} at η = 100 mV) [49], CoP (0.046 s^{-1} at η = 100 mV) [53], MoP (0.024 s^{-1} at η = 100 mV) [54], MoN_1C_2 (0.84 s^{-1} at η = 150 mV) [55], and P-1T MoS_2 (0.5 s^{-1} at η = 153 mV) [56].

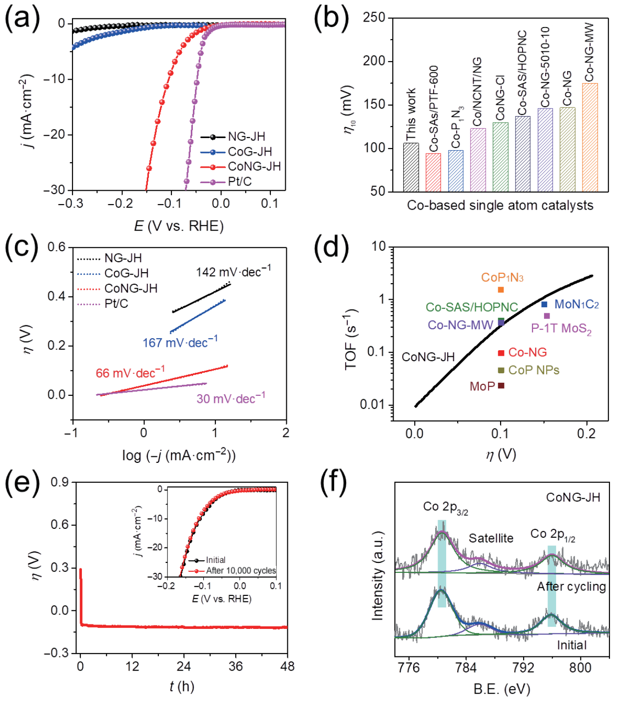

Figure 4 Electrocatalytic performance toward HER. (a) LSV curves after *iR* and background correction for CoNG-JH, CoG-JH, NG-JH and 20 wt.% Pt/C at the scan rate of 1 mV·s^{-1} in 0.5 M H_2SO_4. (b) Comparison of HER activities in terms of η_{10} between CoNG-JH and the state-of-the-art Co-based SACs reported recently. (c) Tafel slopes for CoNG-JH, CoG-JH, NG-JH and Pt/C. (d) TOF values of CoNG-JH at different overpotentials along with other recently reported catalysts. (e) Stability of CoNG-JH evaluated by the η–t curve at the current density of 10 mA·cm^{-2} for 48 h. The inset curve shows the polarization curves of CoNG-JH before and after 10,000 CV cycles. (f) High-resolution XPS Co 2p spectra of CoNG-JH before and after accelerated cycling.

In addition to the catalytic activity, the electrocatalytic stability is also a very important factor in practical applications. Figure 4(e) shows the stability test of CoNG-JH by the galvanostatic technique at the current density of 10 mA·cm^{-2} and it exhibits a slightly increased overpotential by ~ 10 mV after 48 h, suggesting the excellent stability of CoNG-JH. Additionally, cyclic stability tests up to 10,000 CV cycles confirm that CoNG-JH is electrocatalytically stable (inset of Fig. 4(e)). To probe the possible structural and compositional changes induced by long-term stability test, CoNG-JH after accelerated cycling was characterized by SEM, ICP-MS, ADF-STEM and XPS, as displayed in Fig. 4(f), Figs. S10 and S11, and Table S2 in the ESM. The cycling operation did not change the interconnected porous structures, Co content and atomic Co dispersion, revealing the excellent stability of morphology and atomic structure of CoNG-JH. Co 2p XPS spectrum for CoNG-JH after cycling maintains two dominant peaks at 780.5 and 795.9 eV ascribed to CoN_x without metallic Co-related peaks, suggesting the stable existence of the atomically dispersed CoN_x moieties. Therefore, the excellent electrocatalytic stability of CoNG-JH can be attributed to the robust interconnected porous structures conducive to mass transport and exposure of active sites and the chemically stable CoN_x moieties.

3 Conclusions

In summary, we have reported a rapid and facile Joule heating approach to successfully synthesize a self-supported graphene-based Co-N-C single-atom monolith. The ultrafast Joule heating process ensures the rapid formation of atomic CoN_x sites, and the instantaneous quenching avoids the extended heating-induced atom aggregation. The CoN_x moieties serve as HER-active centers, while the three-dimensional hierarchically porous architecture promotes the mass transfer efficiency. Benefiting from these advantageous features, the as-prepared monolithic CoNG-JH electrode exhibits high activity and stability for electrochemical hydrogen generation. The ultrafast Joule heating/quenching procedure enables the rapid and stable dispersion of single atoms on graphene, which provides an economical and highly efficient route for carbon-based single-atom manufacturing for potential practical applications.

4 Experimental

4.1 Preparation of CoNG-JH

Graphene oxide (GO) was firstly prepared by thermal expansion and oxidation of graphite flakes (50 mesh) based on the modified Hummers' method [57]. The amine-functionalized GO (AGO) was prepared through adding dropwise 1 mL $NH_3{\cdot}H_2O$ solution (30%) into 10 mL GO aqueous suspension (2 $mg{\cdot}mL^{-1}$) with magnetic stirring, after which the homogeneous mixture was sealed in a 50 mL autoclave for 5 h at 70 °C. After cooling to room temperature, the purified AGO was obtained after repeated water washing and centrifugation to remove the excessive $NH_3{\cdot}H_2O$. Then, the AGO solution (20 mg) was mixed with 100 μL $CoCl_2{\cdot}6H_2O$ (3 $mg{\cdot}mL^{-1}$) and ethanol (volume ratio in mixture: 10 vol.%) by magnetic stirring for 2 h, after which the homogeneous mixture (weight ratio of AGO : Co = 269 : 1) was sealed in a 100 mL autoclave for 12 h at 120 °C. After hydrothermal process, the self-assembled hydrogel was sliced into thin monolithic film with desired thickness and then freeze-dried to obtain Co^{2+}-containing AGO (CoAGO) aerogel. Subsequently, the CoAGO aerogel precursor was subjected to an ultrafast electrically-triggered Joule heating process for 2 s in NH_3 (100 sccm) to achieve the final catalyst CoNG-JH. The synthesis process of control catalysts NG-JH/CoG-JH was similar to that of CoNG-JH except that no cobalt salts were added for NG-JH and no nitrogen sources were introduced for CoG-JH by using GO as precursor and Ar (100 sccm) as the carrier gas during the Joule heating process.

4.2 Rapid Joule heating method

The aforementioned CoAGO aerogel precursors were suspended on glass slides by connecting each monolithic film with appropriate size (1.5 cm × 0.5 cm) to two copper electrodes with silver paste. The Joule heating synthesis of the monolithic films was conducted in a quartz tank with flowing NH_3 or Ar atmosphere. The electrical pulse process with transient heating/cooling was achieved by the sweep function of Keithley 2425 SourceMeter as the external power source. After optimization, the current source of 1 A and heating duration of 2 s were selected as the optimal condition of electrical pulse. The shorter heating duration (< 2 s) can result in partial lighting of the monolithic films because of a limited amount of time for heat to dissipate throughout the entire sample, while the longer heating duration can result in the extended heating-induced atom aggregation.

4.3 Material characterizations

The structure and morphology of catalysts were investigated by XRD (Bruker, D8 Advance), Raman spectrometer (Renishaw inVia-reflex, 532 nm laser), FT-IR (Bruker, Vertex 70) and SEM (COXEM EM-30 Plus). The specific surface area and pore size distribution were measured by N_2 adsorption-desorption experiment on Micromeritics ASAP 2460. The metal content of samples was measured by ICP-MS (Agilent 7900). The elemental compositions and chemical states of samples were investigated by XPS (Kratos Axis Supra). The HAADF-STEM imaging and EDS elemental mapping were conducted on FEI-Titan Cubed Themis G2 300 equipped with an energy dispersive X-ray spectroscopy.

4.4 Electrochemical measurements

The electrochemical measurements were carried out in 0.5 M H_2SO_4 electrolyte on a standard three-electrode electrochemical workstation (CHI 760E). The graphite rod and $Hg/HgSO_4$, K_2SO_4 (sat) (Wuhan Gaoss Union Co. Ltd.) were used as the counter electrode and reference electrode, respectively. The monolithic electrodes (CoNG-JH, NG-JH and CoG-JH) were directly used as the working electrodes with the optimal thickness of 1.5–2 mm and average areal mass loading of 1.0 $mg{\cdot}cm^{-2}$. The electrode of CoNG-JH-slurry was prepared by a drop-casting method. In detail, 1 mg CoNG-JH catalyst, 250 μL ethanol and 20 μL 5 wt.% Nafion solution were mixed with sonication, and the obtained catalyst ink was then drop-casted on glassy carbon electrode (diameter = 5 mm) to give an optimized mass loading of 0.4 $mg{\cdot}cm^{-2}$. The CV and LSV curves were collected at the scan rate of 20 and 1 $mV{\cdot}s^{-1}$, respectively. The measured potentials against reference electrode were converted to reversible hydrogen electrode (RHE) according to $E_{RHE} = E_{Hg/HgSO_4} + 0.707$ V based on the calibration results. All polarization curves were subjected to background and *iR* correction, as illustrated in Fig. S4 in the ESM. EIS was measured by AC impedance spectroscopy in potentiostatic mode at the overpotential of 150 mV, applying a sinusoidal voltage with an amplitude of 5 mV and scanning frequency from 1,000 kHz to 0.01 Hz. The electrocatalytic stability for the CoNG-JH was evaluated by comparing the LSV curve before and after 10,000 CV cycles and the η–t curve testing at a current density of 10 $mA{\cdot}cm^{-2}$.

Acknowledgements

H. L. F. acknowledges financial support from the National Natural Science Foundation of China (No. 51902099), Hunan high-level talent gathering project (No. 2019RS1021), Fundamental Research Funds for the Central Universities (No. 531119200087).

Electronic Supplementary Material: Supplementary material (additional figures and tables) is available in the online version of this article at https://doi.org/10.1007/s12274-021-4046-z.

References

[1] Yang, X. F.; Wang, A. Q.; Qiao, B. T.; Li, J.; Liu, J. Y.; Zhang, T. Single-atom catalysts: A new frontier in heterogeneous catalysis. *Acc. Chem. Res.* **2013**, *46*, 1740–1748.

[2] Chen, Y. J.; Ji, S. F.; Sun, W. M.; Lei, Y. P.; Wang, Q. C.; Li, A.; Chen, W. X.; Zhou, G.; Zhang, Z. D.; Wang, Y. et al. Engineering the atomic interface with single platinum atoms for enhanced photocatalytic hydrogen production. *Angew. Chem.* **2020**, *132*, 1311–1317.

[3] Yang, J. R.; Li, W. H.; Wang, D. S.; Li, Y. D. Single-atom materials: Small structures determine macroproperties. *Small Struct.* **2021**, *2*, 2000051.

[4] Chen, Y. J.; Ji, S. F.; Chen, C.; Peng, Q.; Wang, D. S.; Li, Y. D. Single-atom catalysts: Synthetic strategies and electrochemical applications. *Joule* **2018**, *2*, 1242–1264.

[5] Han, A. L.; Wang, X. J.; Tang, K.; Zhang, Z. D.; Ye, C. L.; Kong, K. J.; Hu, H. B.; Zheng, L. R.; Jiang, P.; Zhao, C. X. et al. An adjacent atomic platinum site enables single-atom iron with high oxygen reduction reaction performance. *Angew. Chem., Int. Ed.* **2021**, *60*, 19262–19271.

[6] Lei, Y. P.; Wang, Y. C.; Liu, Y.; Song, C. Y.; Li, Q.; Wang, D. S.; Li, Y. D. Designing atomic active centers for hydrogen evolution electrocatalysts. *Angew. Chem., Int. Ed.* **2020**, *59*, 20794–20812.

[7] Yang, J. R.; Li, W. H.; Tan, S. D.; Xu, K. N.; Wang, Y.; Wang, D. S.; Li, Y. D. The electronic metal-support interaction directing the design of single atomic site catalysts: Achieving high efficiency towards hydrogen evolution. *Angew. Chem.* **2021**, *133*, 19233–19239.

[8] Baby, A.; Trovato, L.; Di Valentin, C. Single atom catalysts (SAC) trapped in defective and nitrogen-doped graphene supported on metal substrates. *Carbon* **2021**, *174*, 772–788.

[9] Bie, C. B.; Yu, H. G.; Cheng, B.; Ho, W. K.; Fan, J. J.; Yu, J. G. Design, fabrication, and mechanism of nitrogen-doped graphene-based photocatalyst. *Adv. Mater.* **2021**, *33*, 2003521.

[10] Jing, H. Y.; Zhu, P.; Zheng, X. B.; Zhang, Z. D.; Wang, D. S.; Li, Y. D. Theory-oriented screening and discovery of advanced energy transformation materials in electrocatalysis. *Adv. Powder Mater.*, in press, DOI: 10.1016/j.apmate.2021.10.004.

[11] Fei, H. L.; Dong, J. C.; Chen, D. L.; Hu, T. D.; Duan, X. D.; Shakir, I.; Huang, Y.; Duan, X. F. Single atom electrocatalysts supported on graphene or graphene-like carbons. *Chem. Soc. Rev.* **2019**, *48*, 5207–5241.

[12] He, Y. H.; Liu, S. W.; Priest, C.; Shi, Q. R.; Wu, G. Atomically dispersed metal-nitrogen-carbon catalysts for fuel cells: Advances in catalyst design, electrode performance, and durability improvement. *Chem. Soc. Rev.* **2020**, *49*, 3484–3524.

[13] Fei, H. L.; Dong, J. C.; Feng, Y. X.; Allen, C. S.; Wan, C. Z.; Volosskiy, B.; Li, M. F.; Zhao, Z. P.; Wang, Y. L.; Sun, H. T. et al. General synthesis and definitive structural identification of MN_4C_4 single-atom catalysts with tunable electrocatalytic activities. *Nat. Catal.* **2018**, *1*, 63–72.

[14] Pan, Y.; Chen, Y. J.; Wu, K. L.; Chen, Z.; Liu, S. J.; Cao, X.; Cheong, W. C.; Meng, T.; Luo, J.; Zheng, L. R. et al. Regulating the coordination structure of single-atom $Fe\text{-}N_xC_y$ catalytic sites for benzene oxidation. *Nat. Commun.* **2019**, *10*, 4290.

[15] Guan, J. Q.; Duan, Z. Y.; Zhang, F. X.; Kelly, S. D.; Si, R.; Dupuis, M.; Huang, Q. G.; Chen, J. Q.; Tang, C. H.; Li, C. Water oxidation on a mononuclear manganese heterogeneous catalyst. *Nat. Catal.* **2018**, *1*, 870–877.

[16] Du, Z. Z.; Chen, X. J.; Hu, W.; Chuang, C. H.; Xie, S.; Hu, A. J.; Yan, W. S.; Kong, X. H.; Wu, X. J.; Ji, H. X. et al. Cobalt in nitrogen-doped graphene as single-atom catalyst for high-sulfur content lithium-sulfur batteries. *J. Am. Chem. Soc.* **2019**, *141*, 3977–3985.

[17] Fei, H. L.; Dong, J. C.; Wan, C. Z.; Zhao, Z. P.; Xu, X.; Lin, Z. Y.; Wang, Y. L.; Liu, H. T.; Zang, K. T.; Luo, J. et al. Microwave-assisted rapid synthesis of graphene-supported single atomic metals. *Adv. Mater.* **2018**, *30*, 1802146.

[18] Lacey, S. D.; Dong, Q.; Huang, Z. N.; Luo, J. R.; Xie, H.; Lin, Z. W.; Kirsch, D. J.; Vattipalli, V.; Povinelli, C.; Fan, W. et al. Stable multimetallic nanoparticles for oxygen electrocatalysis. *Nano Lett.* **2019**, *19*, 5149–5158.

[19] Xie, P. F.; Yao, Y. G.; Huang, Z. N.; Liu, Z. Y.; Zhang, J. L.; Li, T. Y.; Wang, G. F.; Shahbazian-Yassar, R.; Hu, L. B.; Wang, C. Highly efficient decomposition of ammonia using high-entropy alloy catalysts. *Nat. Commun.* **2019**, *10*, 4011.

[20] Yao, Y. G.; Huang, Z. N.; Xie, P. F.; Lacey, S. D.; Jacob, R. J.; Xie, H.; Chen, F. J.; Nie, A. M.; Pu, T. C.; Rehwoldt, M. et al. Carbothermal shock synthesis of high-entropy-alloy nanoparticles. *Science* **2018**, *359*, 1489–1494.

[21] Yao, Y. G.; Huang, Z. N.; Xie, P. F.; Li, T. Y.; Lacey, S. D.; Jiao, M. L.; Xie, H.; Fu, K. K.; Jacob, R. J.; Kline, D. J. et al. Ultrafast, controllable synthesis of sub-nano metallic clusters through defect engineering. *ACS Appl. Mater. Interfaces* **2019**, *11*, 29773–29779.

[22] Yao, Y. G.; Huang, Z. N.; Xie, P. F.; Wu, L. P.; Ma, L.; Li, T. Y.; Pang, Z. Q.; Jiao, M. L.; Liang, Z. Q.; Gao, J. L. et al. High temperature shockwave stabilized single atoms. *Nat. Nanotechnol.* **2019**, *14*, 851–857.

[23] Jin, Q. Y.; Ren, B. W.; Cui, H.; Wang, C. X. Nitrogen and cobalt co-doped carbon nanotube films as binder-free trifunctional electrode for flexible zinc-air battery and self-powered overall water splitting. *Appl. Catal. B: Environ.* **2021**, *283*, 119643.

[24] Ma, T. Y.; Dai, S.; Qiao, S. Z. Self-supported electrocatalysts for advanced energy conversion processes. *Mater. Today* **2016**, *19*, 265–273.

[25] Cai, G. R.; Zhang, W.; Jiao, L.; Yu, S. H.; Jiang, H. L. Template-directed growth of well-aligned MOF arrays and derived self-supporting electrodes for water splitting. *Chem* **2017**, *2*, 791–802.

[26] Son, H. J.; Kim, M. J.; Ahn, S. H. Monolithic Co-N-C membrane integrating Co atoms and clusters as a self-supporting multi-functional electrode for solid-state zinc-air batteries and self-powered water splitting. *Chem. Eng. J.* **2021**, *414*, 128739.

[27] Wang, Y. Q.; Zou, Y. Q.; Tao, L.; Wang, Y. Y.; Huang, G.; Du, S. Q.; Wang, S. Y. Rational design of three-phase interfaces for electrocatalysis. *Nano Res.* **2019**, *12*, 2055–2066.

[28] Xie, W. F.; Song, Y. K.; Li, S. J.; Li, J. B.; Yang, Y. S.; Liu, W.; Shao, M. F.; Wei, M. Single-atomic-Co electrocatalysts with self-supported architecture toward oxygen-involved reaction. *Adv. Funct. Mater.* **2019**, *29*, 1906477.

[29] Pan, Z. Y.; Tang, Z.; Zhan, Y. Z.; Sun, D. Three-dimensional porous $CoNiO_2$@reduced graphene oxide nanosheet arrays/nickel foam as a highly efficient bifunctional electrocatalyst for overall water splitting. *Tungsten* **2020**, *2*, 390–402.

[30] Lv, Z. P.; Ma, W. S.; Wang, M.; Dang, J.; Jian, K. L.; Liu, D.; Huang, D. J. Co-constructing interfaces of multiheterostructure on MXene ($Ti_3C_2T_x$)-modified 3D self-supporting electrode for ultraefficient electrocatalytic HER in alkaline media. *Adv. Funct. Mater.* **2021**, *31*, 2102576.

[31] Zhang, L. L.; Wang, Y. J.; Niu, Z. Q.; Chen, J. Single atoms on graphene for energy storage and conversion. *Small Methods* **2019**, *3*, 1800443.

[32] Voiry, D.; Yang, J.; Kupferberg, J.; Fullon, R.; Lee, C.; Jeong, H. Y.; Shin, H. S.; Chhowalla, M. High-quality graphene via microwave reduction of solution-exfoliated graphene oxide. *Science* **2016**, *353*, 1413–1416.

[33] Liang, J.; Jiao, Y.; Jaroniec, M.; Qiao, S. Z. Sulfur and nitrogen dual-doped mesoporous graphene electrocatalyst for oxygen reduction with synergistically enhanced performance. *Angew. Chem., Int. Ed.* **2012**, *51*, 11496–11500.

[34] Xia, W.; Tang, J.; Li, J. J.; Zhang, S. H.; Wu, K. C. W.; He, J. P.; Yamauchi, Y. Defect-rich graphene nanomesh produced by thermal exfoliation of metal-organic frameworks for the oxygen reduction reaction. *Angew. Chem., Int. Ed.* **2019**, *58*, 13354–13359.

[35] Zhao, X. J.; Pachfule, P.; Li, S.; Langenhahn, T.; Ye, M. Y.; Schlesiger, C.; Praetz, S.; Schmidt, J.; Thomas, A. Macro/microporous covalent organic frameworks for efficient electrocatalysis. *J. Am. Chem. Soc.* **2019**, *141*, 6623–6630.

[36] Liu, J. J.; Gong, Z. C.; Allen, C.; Ge, W.; Gong, H. S.; Liao, J. W.; Liu, J. B.; Huang, K.; Yan, M. M.; Liu, R. et al. Edge-hosted $Fe\text{-}N_3$ sites on a multiscale porous carbon framework combining high

intrinsic activity with efficient mass transport for oxygen reduction. *Chem Catal.* **2021**, *1*, 1291–1307.

[37] Ma, Y. F.; Chen, M.; Geng, H. B.; Dong, H. F.; Wu, P.; Li, X. M.; Guan, G. Q.; Wang, T. J. Synergistically tuning electronic structure of porous β-Mo_2C spheres by Co doping and Mo-vacancies defect engineering for optimizing hydrogen evolution reaction activity. *Adv. Funct. Mater.* **2020**, *30*, 2000561.

[38] Yang, L.; Lv, Y. L.; Cao, D. P. Co, N-codoped nanotube/graphene 1D/2D heterostructure for efficient oxygen reduction and hydrogen evolution reactions. *J. Mater. Chem. A* **2018**, *6*, 3926–3932.

[39] Jia, Y.; Zhang, L. Z.; Zhuang, L. Z.; Liu, H. L.; Yan, X. C.; Wang, X.; Liu, J. D.; Wang, J. C.; Zheng, Y. R.; Xiao, Z. H. et al. Identification of active sites for acidic oxygen reduction on carbon catalysts with and without nitrogen doping. *Nat. Catal.* **2019**, *2*, 688–695.

[40] Tavakkoli, M.; Flahaut, E.; Peljo, P.; Sainio, J.; Davodi, F.; Lobiak, E. V.; Mustonen, K.; Kauppinen, E. I. Mesoporous single-atom-doped graphene-carbon nanotube hybrid: Synthesis and tunable electrocatalytic activity for oxygen evolution and reduction reactions. *ACS Catal.* **2020**, *10*, 4647–4658.

[41] Lu, Q.; Wu, H.; Zheng, X. R.; Chen, Y. N.; Rogach, A. L.; Han, X. P.; Deng, Y. D.; Hu, W. B. Encapsulating cobalt nanoparticles in interconnected N-doped hollow carbon nanofibers with enriched Co-N-C moiety for enhanced oxygen electrocatalysis in Zn-air batteries. *Adv. Sci.* **2021**, *8*, 2101438.

[42] Fei, H. L.; Dong, J. C.; Arellano-Jiménez, M. J.; Ye, G. L.; Kim, N. D.; Samuel, E. L. G.; Peng, Z. W.; Zhu, Z.; Qin, F.; Bao, J. M. et al. Atomic cobalt on nitrogen-doped graphene for hydrogen generation. *Nat. Commun.* **2015**, *6*, 8668.

[43] Liu, R.; Gong, Z. C.; Liu, J. B.; Dong, J. C.; Liao, J. W.; Liu, H.; Huang, H. K.; Liu, J. J.; Yan, M. M.; Huang, K. et al. Design of aligned porous carbon films with single-atom Co-N-C sites for high-current-density hydrogen generation. *Adv. Mater.* **2021**, *33*, e2103533.

[44] Wang, X. Q.; Chen, Z.; Zhao, X. Y.; Yao, T.; Chen, W. X.; You, R.; Zhao, C. M.; Wu, G.; Wang, J.; Huang, W. X. et al. Regulation of coordination number over single Co sites: Triggering the efficient electroreduction of CO_2. *Angew. Chem., Int. Ed.* **2018**, *57*, 1944–1948.

[45] Faber, M. S.; Dziedzic, R.; Lukowski, M. A.; Kaiser, N. S.; Ding, Q.; Jin, S. High-performance electrocatalysis using metallic cobalt pyrite (CoS_2) micro- and nanostructures. *J. Am. Chem. Soc.* **2014**, *136*, 10053–10061.

[46] Cao, L. L.; Luo, Q. Q.; Liu, W.; Lin, Y.; Liu, X. K.; Cao, Y. J.; Zhang, W.; Wu, Y. E.; Yang, J. L.; Yao, T. et al. Identification of single-atom active sites in carbon-based cobalt catalysts during electrocatalytic hydrogen evolution. *Nat. Catal.* **2019**, *2*, 134–141.

[47] Liang, H. W.; Brüller, S.; Dong, R. H.; Zhang, J.; Feng, X. L.; Müllen, K. Molecular metal-N_x centres in porous carbon for electrocatalytic hydrogen evolution. *Nat. Commun.* **2015**, *6*, 7992.

[48] Yi, J. D.; Xu, R.; Chai, G. L.; Zhang, T.; Zang, K. T.; Nan, B.; Lin, H.; Liang, Y. L.; Lv, J. Q.; Luo, J. et al. Cobalt single-atoms anchored on porphyrinic triazine-based frameworks as bifunctional electrocatalysts for oxygen reduction and hydrogen evolution reactions. *J. Mater. Chem. A* **2019**, *7*, 1252–1259.

[49] Wan, J. W.; Zhao, Z. H.; Shang, H. S.; Peng, B.; Chen, W. X.; Pei, J. J.; Zheng, L. R.; Dong, J. C.; Cao, R.; Sarangi, R. et al. *In situ* phosphatizing of triphenylphosphine encapsulated within metal-organic frameworks to design atomic Co_1-P_1N_3 interfacial structure for promoting catalytic performance. *J. Am. Chem. Soc.* **2020**, *142*, 8431–8439.

[50] Wan, G.; Yang, C.; Zhao, W. P.; Li, Q. R.; Wang, N.; Li, T.; Zhou, H.; Chen, H. R.; Shi, J. L. Anion-regulated selective generation of cobalt sites in carbon: Toward superior bifunctional electrocatalysis. *Adv. Mater.* **2017**, *29*, 1703436.

[51] Sun, T. T.; Zhao, S.; Chen, W. X.; Zhai, D.; Dong, J. C.; Wang, Y.; Zhang, S. L.; Han, A. J.; Gu, L.; Yu, R. et al. Single-atomic cobalt sites embedded in hierarchically ordered porous nitrogen-doped carbon as a superior bifunctional electrocatalyst. *Proc. Natl. Acad. Sci. USA* **2018**, *115*, 12692–12697.

[52] Zhang, Y. J.; Li, W. F.; Lu, L. H.; Song, W. G.; Wang, C. R.; Zhou, L. S.; Liu, J. H.; Chen, Y.; Jin, H. Y.; Zhang, Y. G. Tuning active sites on cobalt/nitrogen doped graphene for electrocatalytic hydrogen and oxygen evolution. *Electrochim. Acta* **2018**, *265*, 497–506.

[53] Popczun, E. J.; Read, C. G.; Roske, C. W.; Lewis, N. S.; Schaak, R. E. Highly active electrocatalysis of the hydrogen evolution reaction by cobalt phosphide nanoparticles. *Angew. Chem., Int. Ed.* **2014**, *53*, 5427–5430.

[54] Kibsgaard, J.; Jaramillo, T. F. Molybdenum phosphosulfide: An active, acid-stable, earth-abundant catalyst for the hydrogen evolution reaction. *Angew. Chem., Int. Ed.* **2014**, *53*, 14433–14437.

[55] Chen, W. X.; Pei, J. J.; He, C. T.; Wan, J. W.; Ren, H. L.; Zhu, Y. Q.; Wang, Y.; Dong, J. C.; Tian, S. B.; Cheong, W. C. et al. Rational design of single molybdenum atoms anchored on N-doped carbon for effective hydrogen evolution reaction. *Angew. Chem., Int. Ed.* **2017**, *56*, 16086–16090.

[56] Yin, Y.; Han, J. C.; Zhang, Y. M.; Zhang, X. H.; Xu, P.; Yuan, Q.; Samad, L.; Wang, X. J.; Wang, Y.; Zhang, Z. H. et al. Contributions of phase, sulfur vacancies, and edges to the hydrogen evolution reaction catalytic activity of porous molybdenum disulfide nanosheets. *J. Am. Chem. Soc.* **2016**, *138*, 7965–7972.

[57] Marcano, D. C.; Kosynkin, D. V.; Berlin, J. M.; Sinitskii, A.; Sun, Z. Z.; Slesarev, A.; Alemany, L. B.; Lu, W.; Tour, J. M. Improved synthesis of graphene oxide. *ACS Nano* **2010**, *4*, 4806–4814.